Title

Direct Observation of the Local Reaction Environment during the Electrochemical Reduction of CO2

Permalink

https://escholarship.org/uc/item/1h06f3d4

Author

Bell, AT

Publication Date

2021-10-17

DOI

10.1021/jacs.8b04058

Peer reviewed

Direct Observation of the Local Reaction Environment during the Electrochemical Reduction of CO$_2$

Ezra L. Clark[†,‡] and Alexis T. Bell*[,†,‡]

†Joint Center for Artificial Photosynthesis, Lawrence Berkeley National Laboratory, Berkeley, California 94720, United States
‡Department of Chemical and Biomolecular Engineering, University of California, Berkeley, California 94720, United States

S *Supporting Information*

ABSTRACT: The electrochemical reduction of carbon dioxide is sensitive to electrolyte polarization, which causes gradients in pH and the concentration of carbon dioxide to form near the cathode surface. It is desirable to measure the concentration of reaction-relevant species in the immediate vicinity of the cathode because the intrinsic kinetics of carbon dioxide reduction depend on the composition of the local reaction environment. Meeting this objective has proven difficult because conventional analytical methods only sample products from the bulk electrolyte. In this study, we describe the use of differential electrochemical mass spectrometry to measure the concentration of carbon dioxide and reaction products in the immediate vicinity of the cathode surface. This capability is achieved by coating the electrocatalyst directly onto the pervaporation membrane used to transfer volatile species into the mass spectrometer, thereby enabling species to be sampled directly from the electrode–electrolyte interface. This approach has been used to investigate hydrogen evolution and carbon dioxide reduction over Ag and Cu. We find that the measured CO$_2$ reduction activity of Ag agrees well with what is measured by gas chromatography of the effluent from an H-cell operated with the same catalyst and electrolyte. A distinct advantage of our approach is that it enables observation of the depletion of carbon dioxide near the cathode surface due to reaction with hydroxyl anions evolved at the cathode surface, something that cannot be done using conventional analytical techniques. We also demonstrate that the influence of this relatively slow chemical reaction can be minimized by evaluating electrocatalytic activity during a rapid potential sweep, thereby enabling measurement of the intrinsic kinetics. For CO$_2$ reduction over Cu, nine products can be observed simultaneously in real time. A notable finding is that the abundance of aldehydes relative to alcohols near the cathode surface is much higher than that observed in the bulk electrolyte. It is also observed that for increasingly cathodic potentials the relative abundance of ethanol increases at the expense of propionaldehyde. These findings suggest that acetaldehyde is a precursor to ethanol and propionaldehyde and that propionaldehyde is a precursor to *n*-propanol.
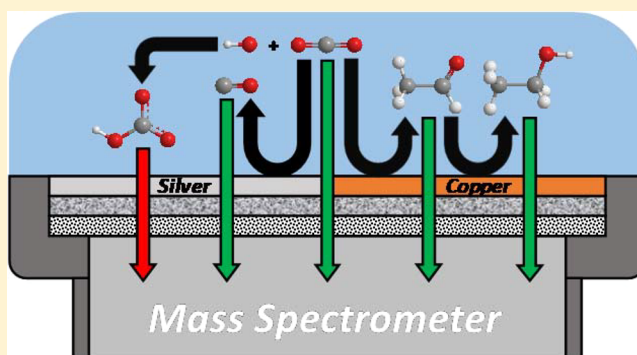
INTRODUCTION

Fuels and commodity chemicals can potentially be produced by the electrochemical reduction of carbon dioxide (CO$_2$).[1−3] The product distribution obtained is highly dependent on the composition of both the metal used as the cathode and the reaction environment in the immediate vicinity of its surface. For example, silver (Ag) produces carbon monoxide (CO) almost exclusively, while copper (Cu) is the only known electrocatalyst capable of producing hydrocarbons and alcohols with high Faradaic efficiency.[4,5] Recent theoretical studies have shown that as the current density increases, electrolyte polarization occurs due to inadequate mass transfer to and from the electrode surface. As a result, the pH and CO$_2$ concentration near the cathode surface deviate significantly from those in the bulk of the electrolyte.[6,7] Determining the extent to which the observed electrocatalytic activity is influenced by concentration polarization is difficult because conventional analytical techniques sample species from the gas-

phase effluent and the bulk electrolyte. Additionally, there is currently little experimental evidence to support any of the proposed mechanisms by which CO$_2$ is reduced to multicarbon products over Cu. For example, it has been hypothesized that aldehydes are intermediates to the corresponding alcohols.[8] While this hypothesis is supported by the observation that the acetaldehyde concentration quickly saturates during prolonged electrolysis and that the electrochemical reduction of these aldehydes yields the corresponding alcohols,[9,10] these data are not sufficient to conclude that aldehydes are intermediates in the reduction of CO$_2$ to either ethanol or *n*-propanol over Cu. Therefore, the ability to quantify the composition of the local reaction environment would enable activity trends to be directly related to the catalytically relevant reactant concentration under different operating conditions. Furthermore, it
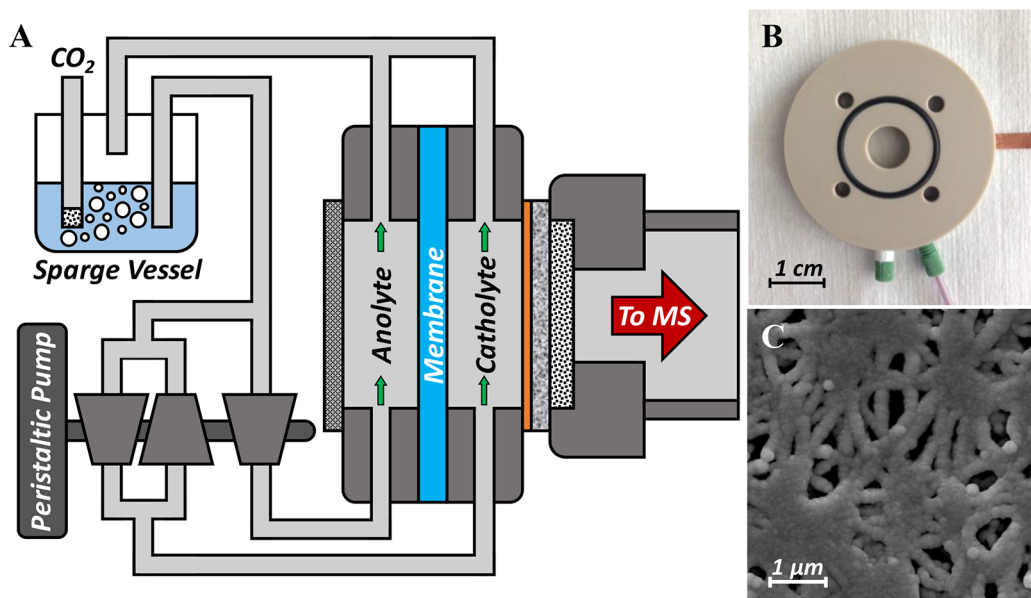
Figure 1. (A) Schematic of the DEMS setup. (B) Photograph of the cathode chamber of the DEMS cell. (C) SEM image of the nanoporous PTFE membrane coated with Ag.

could potentially enable transient intermediate reaction products to be observed, providing insight into the selectivity-determining steps of multicarbon product formation. A promising approach for addressing these issues is differential electrochemical mass spectrometry (DEMS). This analytical technique utilizes pervaporation to continuously collect volatile electrochemical reaction products in real time.[11,12] Unfortunately, DEMS cells for CO_2 reduction are typically configured such that volatile species are sampled form the bulk electrolyte.[9,13] However, by coating the pervaporation membrane with the electrocatalyst, volatile species at the electrode–electrolyte interface can be sampled.[11,12] Furthermore, by colocating the electrocatalyst and the point of product sampling, the delay time between product generation and detection is minimized and the liquid-phase product collection efficiency is maximized.[11,12]

Here, we report the merits of investigating CO_2 reduction with a DEMS cell that enables reactant and product concentrations to be probed in the immediate vicinity of the cathode. This capability has enabled us to observe the acid–base reaction of CO_2 with hydroxyl anions evolved at the cathode surface and demonstrate that the influence of this relatively slow chemical reaction on the measured activity of Ag can be minimized by conducting product analysis during a rapid potential sweep. Furthermore, we have been able to probe the effects of electrolyte hydrodynamics on the electrocatalytic activity of Ag and relate the observed changes to differences in the composition of the local reaction environment. We demonstrate a method of signal deconvolution over Cu that enables the continuous observation of nine different reaction products and observe a potential-dependent hysteresis of the product distribution that favors multicarbon product generation during the anodic sweep. Finally, we have discovered that aldehydes are much more abundant than the corresponding alcohols in the immediate vicinity of the Cu cathode, supporting the hypothesis that they are intermediates to more reduced products.

■ EXPERIMENTAL SECTION

Electrochemical Cell. Figure 1 illustrates the DEMS setup. It consists of an electrochemical cell, a set of electrolyte reservoirs, and a peristaltic pump. The electrochemical cell was machined from PEEK and was cleaned by sonication in 20 wt % nitric acid prior to each experiment. The working and counter electrodes are parallel and separated by an anion-conducting membrane (Selemion AMV AGC Inc.). The exposed geometric surface area of the cathode is ~0.5 cm². The anode is a platinum gauze disc (100 mesh, 99.9% Sigma-Aldrich) with an exposed surface area of roughly 2 cm². The working electrode potential was referenced against an Ag/AgCl electrode (Innovative Instruments Inc.) that was calibrated against a homemade standard hydrogen electrode. A 0.05 M Cs_2CO_3 (99.995% Sigma-Aldrich) solution prepared using 18.2 MΩ DI water was used as the electrolyte. Metallic impurities in the as-prepared electrolyte were removed before electrolysis by chelating them with Chelex 100 (Na form, Sigma-Aldrich).[14] Each electrode chamber had an associated electrolyte vessel that was sparged with CO_2 (99.999%, Praxair Inc.) for 30 min prior to and throughout the duration of all electrochemical measurements. Upon saturation with CO_2, the pH of the electrolyte was 6.8, which was maintained throughout the duration of each experiment. The electrolyte from these reservoirs was continuously pumped through the chambers of the electrochemical cell and recycled using a peristaltic pump. The catholyte was pumped using a parallel set of pump cartridges with opposing polarities, which resulted in constant pressure flow.

Electrode Preparation. A nanoporous PTFE membrane (20 nm pore size, Hangzhou Cobetter Filtration Equipment Co.) was used as the pervaporation membrane and electrocatalyst support. The nanoporous PTFE membrane was sonicated in acetone for 30 min, sonicated in methanol for 30 min, rinsed with DI water, dried over N_2, and exposed to UV generated ozone for 5 min to clean the surface prior to sputter deposition. Cu and Ag thin films were deposited onto the nanoporous PTFE membrane using an AJA ATC Orion-5 magnetron sputtering system. Cu (99.999%, Kurt J. Lesker) and Ag (99.999%, Kurt J. Lesker) were deposited at a rate of 1 Å/s to an effective thickness of 400 nm under Ar. This thickness was determined to maximize the CO mass-ion current signal during linear sweep voltammetry over Ag (see SI-1). A scanning electron micrograph of the nanoporous PTFE membrane coated with Ag is shown in Figure 1C.

Electrode Characterization. The bulk crystal structures of the Cu and Ag thin films deposited onto the nanoporous PTFE membrane

were analyzed using a Rigaku Smartlab X-ray diffractometer (XRD). The symmetric out-of-plane diffractograms were acquired using Cu Kα radiation (40 kV, 40 mA). The average crystallite size of the particles comprising the thin films was calculated using the Scherrer equation. Scanning electron micrographs of the Cu and Ag thin films were acquired using an FEI Quanta FEG 250 scanning electron microscope (SEM). The micrographs were acquired using an electron beam energy of 15 kV and a spot size of 3.0 nm.

The near-surface compositions of the Cu and Ag thin films were measured before and after electrolysis using a Kratos Axis Ultra DLD X-ray photoelectron spectrometer (XPS). All spectra were acquired using monochromatized Al Kα radiation (15 kV, 15 mA). Ar sputtering of the sample surface was avoided to prevent the removal of surface contaminants. The kinetic energy scale of the measured spectra was calibrated by setting the C 1s binding energy to 284.8 eV. The same instrument was also used to measure the surface composition of the Cu and Ag thin films before and after electrolysis by ion scattering spectroscopy (ISS). All spectra were acquired using a focused He ion beam (1 kV). No impurities were detected on the electrode surface before or after electrolysis by either XPS or ISS (see SI-2).

Electrochemistry. Electrochemistry was performed using a Biologic VSP-300 potentiostat. All electrochemical measurements were recorded versus the reference electrode and converted to the RHE scale. The working electrode was conditioned prior to experimentation by conducting chronopotentiometry at −20 mA/cm^2 for 30 min. Potentiostatic electrochemical impedance spectroscopy (PEIS) and current interrupt (CI) were used to determine the uncompensated resistance (R_u) of the electrochemical cell (see SI-3). While the potentiostat compensated for 85% of R_u in situ, the last 15% was not corrected because this would result in a potential scale that does not vary linearly with time, making the accurate alignment of the electrochemistry and mass spectrometry erroneous.

The roughness factor of the Ag films deposited onto the nanoporous PTFE membrane were determined relative to an identical film deposited onto a polished Si wafer by taking the ratio of their double layer capacitances. The double layer capacitance of each electrode was measured by conducting cyclic voltammetry in a potential range where no Faradaic processes occur at a series of increasingly rapid scan rates (see SI-4).

Mass Spectrometry. Mass spectra were acquired using a Hiden HPR40 dissolved-species mass spectrometer. An electron energy of 70 eV was used for the ionization of all species with an emission current of 500 μA. All mass-selected product cations were accelerated using a voltage of 3 V and were detected using a secondary electron multiplier with a detector voltage of 1,350 V. The mass spectra of relevant species were measured so that accurate deconvolution of the observed mass spectrum could be conducted (see SI-5).

■ RESULTS AND DISCUSSION

Hydrogen Evolution over Ag. Hydrogen evolution was investigated over Ag in the absence of CO$_2$ to confirm that the measured mass-ion currents are directly proportional to the rates of electrochemical product generation. To this end, a chronopotentiometry staircase was conducted while monitoring the $m/z = 2$ mass-ion current (see SI-6). The linear correlation between the $m/z = 2$ mass-ion current signal and the total current density confirms the quantitative nature of the observed mass-ion currents and demonstrates that the product collection efficiency is independent of the absolute current density. Furthermore, the reproducibility of the H$_2$ calibration curve indicates that the product collection efficiency does not vary with extended operation. The product collection efficiency was estimated to be ~80% by comparing the slope of the H$_2$ calibration curve observed at an electrolyte flow rate of 85 mL/min to that observed under stagnant electrolyte conditions, where complete product collection was assumed to occur.
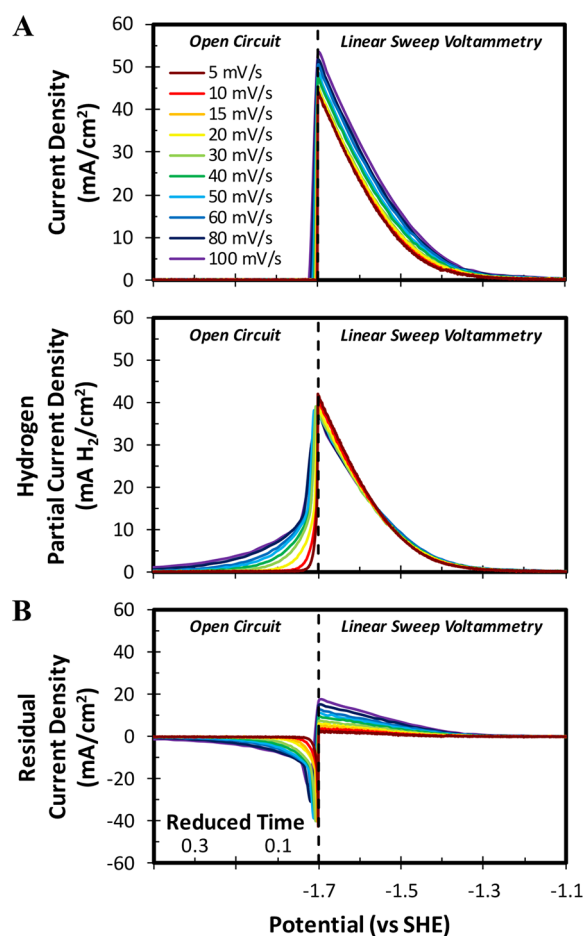

Figure 2. (A) H$_2$ evolution activity of Ag measured during linear sweep voltammetry at a series of increasingly rapid scan rates in 0.1 M CsHCO$_3$ saturated with N$_2$ at a flow rate of 85 mL/min. (B) Difference between the total current density and the observed H$_2$ partial current density. Reduced time is defined as the time elapsed after the terminal potential of the potential scan is reach normalized by the time required to scan through a 1 mV potential window.

Thus, product collection efficiencies remain high despite that electrolyte convection enhances the flux of electrochemical reaction products away from the electrode surface and into the bulk of the electrolyte. The H$_2$ detection limit, defined as the partial current density that results in a mass-ion current signal greater than the standard deviation of the baseline, was determined to be ~40 μA/cm^2 at this flow rate.

The temporal accuracy of product quantification was evaluated by conducting linear sweep voltammetry at rates of 5−100 mV/s while monitoring the $m/z = 2$ mass-ion current. The observed $m/z = 2$ signal was converted into the corresponding H$_2$ partial current density using the calibration curve described above and is shown in Figure 2A. As the scan rate increased, higher current densities were observed at a fixed potential. The increase in the maximum current density was roughly 3 orders of magnitude higher than the current associated with charging the electrochemical double layer (see SI-4). Thus, the increase in the maximum current density is hypothesized to be the result of the suppressed depletion of bicarbonate anions near the cathode surface as the scan rate is increased. The depletion of the bicarbonate anions near the cathode is suppressed at higher scan rates because fewer hydroxyl anions are evolved over the course of the linear
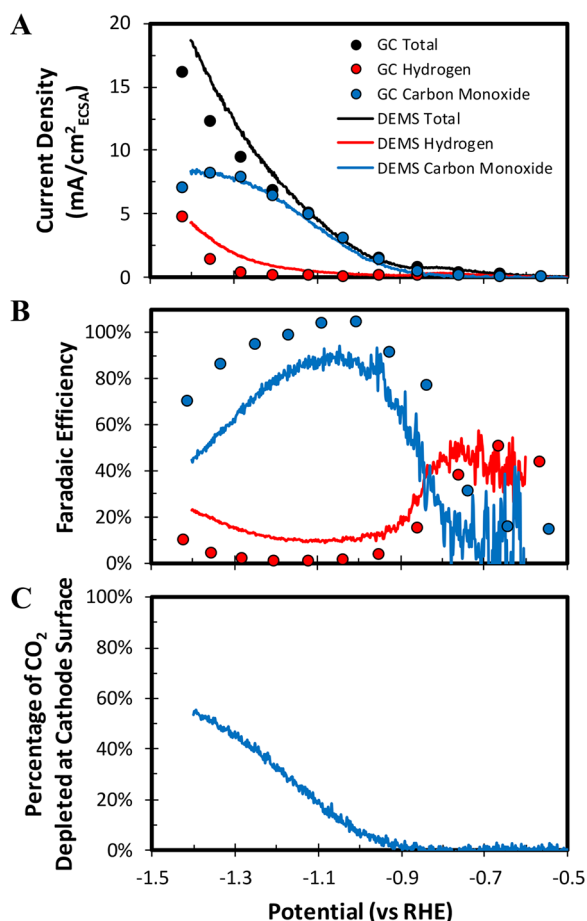
Figure 3. Comparison of the CO_2 reduction activity of Ag measured via GC and DEMS in 0.1 M $CsHCO_3$: (A) ECSA-normalized partial current densities and (B) Faradaic efficiencies. GC measurements were conducted during a chronoamperometry staircase in a traditional H-cell with a CO_2 flow rate of 20 sccm. DEMS measurements were conducted during linear sweep voltammetry at a scan rate of 5 mV/s with an electrolyte flow rate of 85 mL/min. (C) Fraction of CO_2 depleted at the cathode surface as measured by DEMS during linear sweep voltammetry.

Figure 4. (A) CO_2 reduction activity of Ag measured during linear sweep voltammetry at a series of increasingly rapid scan rates in 0.1 M $CsHCO_3$ at a flow rate of 85 mL/min. (B) CO_2 signal ($m/z = 44$) versus CO signal (deconvoluted $m/z = 28$) observed during linear sweep voltammetry over Ag at a series of increasingly rapid scan rates. The dotted line depicts the relationship expected if CO_2 depletion occurs only by the evolution of CO.

potential sweep as the scan rate is increased. Recent work has shown that HCO_3^- anions can serve as a source of adsorbed H atoms (H*) via the reaction: $HCO_3^- + e^- \rightarrow H^* + CO_3^{2-}$. The reason that HCO_3^- anions are an effective source of absorbed H* is that the pK_a of HCO_3^- anions is 3.7 pK_a units lower than that of water (10.3 vs 14), which means that despite the lower concentration of HCO_3^- anions (0.1 M) relative to that of water (55 M), HCO_3^- anions can compete with water as a source of H*.[15]

The difference between the total current density and the observed H_2 partial current density was calculated to determine the scan rate dependence of the quantification error, as shown in Figure 2B. The total fraction of charge passed during the linear potential sweep accounted for by detected H_2 only decreases marginally with scan rate (see SI-7). However, a greater fraction of the H_2 is detected after the scan ends as the scan rate is increased due to the finite time between product generation and detection. This ultimately results in product detection after the terminal potential is reached. However, the observed mass-ion current signal accurately reproduces the voltammogram for scan rates below ~10 mV/s. The exponential decay of the $m/z = 2$ signal is thought to be
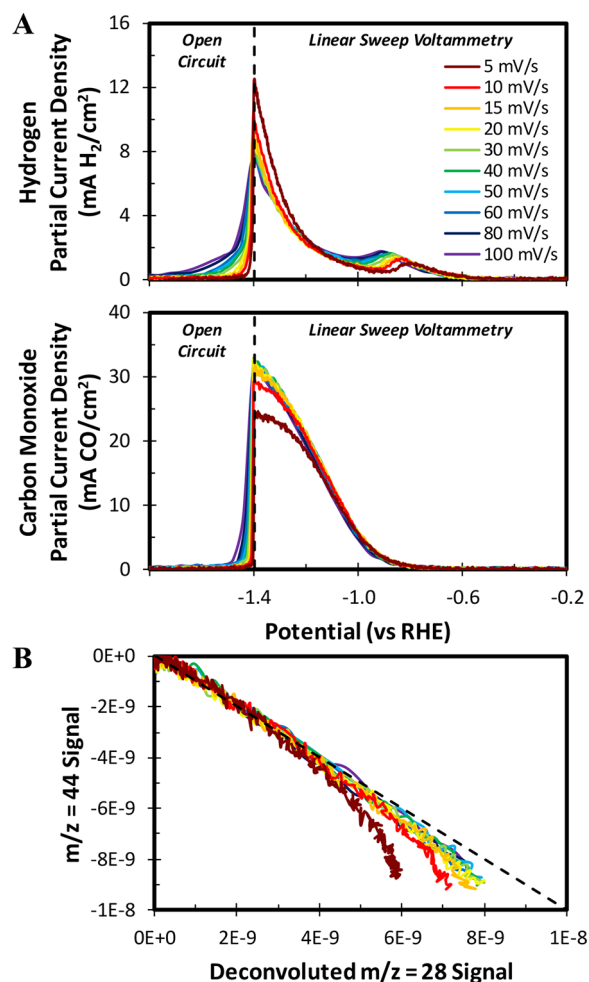
caused by the diffusion of H_2 into the electrolyte and then back toward the pervaporation membrane once the scan has ended. It is notable that this behavior was not observed for other reaction products, which diffuse through water at much slower rates than H_2 (see SI-7).

CO_2 Reduction over Ag. CO_2 reduction was conducted over Ag to validate that the electrocatalytic activity measured by DEMS accurately reproduces what is measured by gas chromatography (GC). Ag is an ideal electrocatalyst for this purpose because it predominantly produces H_2 and CO at all applied potentials.[16,17] The ionization of CO produces some of the same mass fragments as the ionization of CO_2, necessitating deconvolution of the contributions of CO and CO_2 to the observed mass spectrum (see SI-8). CO calibration was conducted in an analogous way as H_2 calibration, except that the mass-ion currents for $m/z = 2$, 28, and 44 were all monitored during the chronopotentiometry staircase (see SI-9). The CO partial current density was assumed to be equivalent to the difference between the total current density and the H_2 partial current density, which was determined using the observed $m/z = 2$ mass-ion current and the H_2 calibration
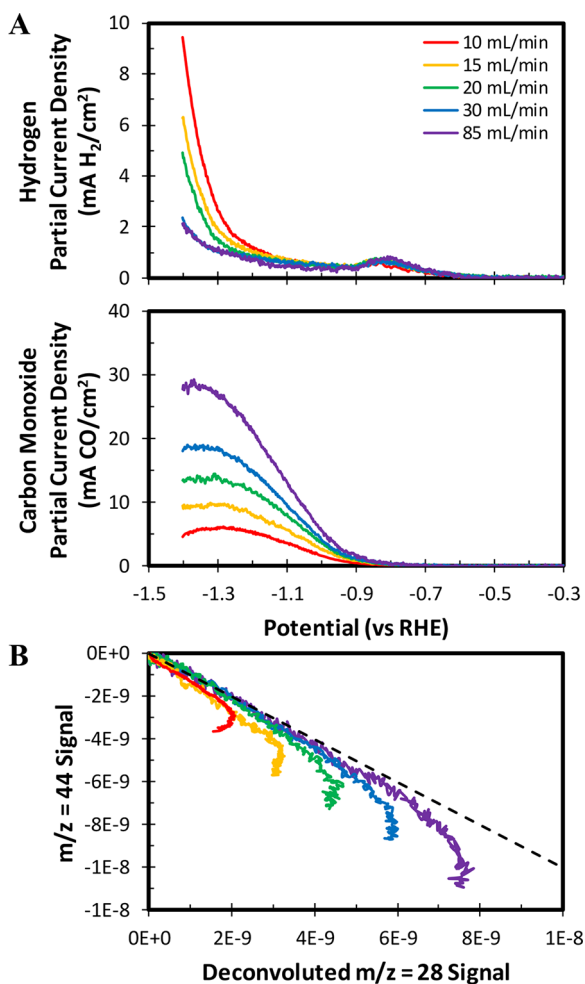
Figure 5. (A) CO_2 reduction activity of Ag measured during linear sweep voltammetry at a scan rate of 5 mV/s in 0.1 M $CsHCO_3$ at different flow rates. (B) CO_2 signal ($m/z = 44$) versus CO signal (deconvoluted $m/z = 28$) observed during linear sweep voltammetry over Ag at different electrolyte flow rates. The dotted line depicts the relationship expected if CO_2 depletion occurs only by the evolution of CO.

curve. The contribution of CO_2 to the observed $m/z = 28$ signal was accounted for using the observed $m/z = 44$ mass-ion current and the measured mass spectrum of CO_2. The resulting linear correlation between the deconvoluted $m/z = 28$ mass-ion current signal and the calculated CO partial current density validates the assumption that the only products evolved at the cathode surface in appreciable quantities under these conditions are H_2 and CO (see SI-9).

Linear sweep voltammetry was conducted at a scan rate of 5 mV/s while monitoring the mass-ion currents for $m/z = 2, 28,$ and 44. The results obtained were analyzed in an analogous fashion and compared to those obtained by analyzing the effluent of an H-cell using gas chromatograph while performing a chronoamperometry staircase over a polycrystalline Ag thin film. As shown in Figure 3A and B, the ECSA-normalized partial current densities and Faradaic efficiencies observed via DEMS and GC match exceptionally well, notwithstanding the fact that the DEMS approach acquires the data nearly 2 orders of magnitude faster than the conventional approach. Furthermore, the DEMS approach enables the extent of CO_2 depletion near the cathode surface to be measured

experimentally, as shown in Figure 3C. Thus, the technique can be used to relate changes in the observed electrocatalytic activity to the composition of the local reaction environment.

To determine if the scan rate impacts the observed electrocatalytic activity and local reaction environment over Ag, linear sweep voltammetry was conducted at increasingly rapid scan rates (see SI-10). As shown in Figure 4A, as the scan rate is increased, the small bump in the H_2 partial current density at roughly −0.8 V vs RHE shifts to more cathodic potentials. This feature is likely caused by the poisoning of surface sites by adsorbed intermediates associated with the reduction of CO_2 to CO. This hypothesis is corroborated by the observation that the H_2 partial current density declines at the onset potential of CO evolution and that spectroscopic studies in the published literature have observed IR absorption bands associated with COOH over polarized Ag cathodes during CO_2 reduction.[18] The maximum in the H_2 partial current wave at roughly −0.8 V vs RHE shifts to more cathodic potentials as the scan rate is increased because these intermediates take a finite time to accumulate on the Ag surface, enabling more cathodic potentials to be reached before they accumulate to a significant extent as the scan rate is increased. Furthermore, as the scan rate is increased from 5 to 20 mV/s, the observed H_2 partial current density decreases, while the observed CO partial current density increases at potentials cathodic of −1 V vs RHE. However, scan rates faster than 20 mV/s do not exhibit any additional changes. The origin of this scan rate dependence was determined by plotting the mass-ion current signal associated with CO_2 as a function of the deconvoluted mass-ion current signal associated with CO measured during each linear potential sweep, as shown in Figure 4B. A linear correlation is observed at low CO generation rates regardless of the scan rate employed, suggesting that a molecule of CO is generated for every molecule of CO_2 consumed. However, at higher rates of CO generation, the local CO_2 concentration is depleted to a greater degree than expected on the basis of the rate of CO generation alone. Furthermore, the magnitude of this excessive depletion increases at a fixed CO generation rate as the scan rate drops below 20 mV/s. These trends cannot be explained in terms of differences in the rates of mass transfer of CO and CO_2 from the electrode surface into the mass spectrometer because both species diffuse through aqueous solutions at nearly identical rates, with diffusion coefficients of 1.92 and 2.03×10^{-5} cm^2/s, respectively. Conversely, these observations suggest that there is a second mode of CO_2 depletion that becomes relevant at potentials cathodic of −1 V vs RHE at scan rates below 20 mV/s. This additional mode of CO_2 depletion is hypothesized to be the reaction of CO_2 with hydroxyl anions evolved at the cathode surface, which produces bicarbonate anions and depletes the local CO_2 concentration.[6,7] The extent to which this reaction depletes the local CO_2 concentration scales with the concentration of hydroxyl anions produced at the cathode surface during the linear potential sweep, which decreases as the scan rate increases. It is important to realize that the intrinsic electrocatalytic activity can only be measured if the extent of concentration polarization is minimized. The DEMS approach accomplishes this by sampling products directly at the electrode−electrolyte interface, thereby enabling product analysis to be conducted continuously during a rapid potential sweep, reducing the depletion of CO_2 by limiting the evolution of hydroxyl anions at the cathode surface.
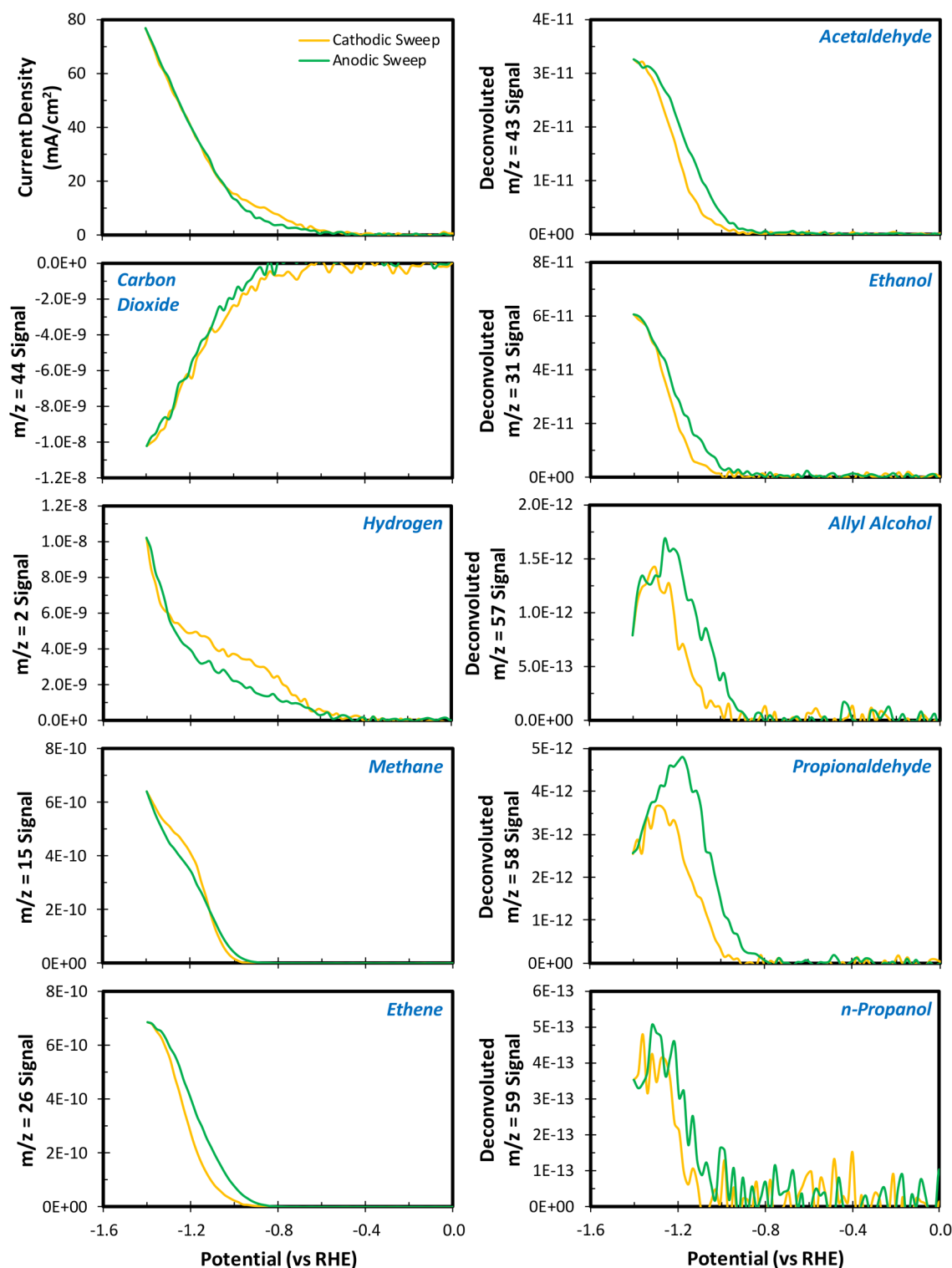
Figure 6. CO_2 reduction activity of Cu measured during cyclic voltammetry at a scan rate of 1 mV/s in 0.1 M $CsHCO_3$ at a flow rate of 85 mL/min. Signals shown in the right-hand panels have been obtained by deconvoluting the total mass-ion current so that only the signal of the primary contributing product is displayed.

To demonstrate the impact that the rate of mass transfer to the cathode surface has on the observed electrocatalytic activity and local reaction environment over Ag, linear sweep voltammetry was conducted at a series of increasingly rapid electrolyte flow rates. As the electrolyte flow rate is increased, the thickness of the hydrodynamic and mass-transfer boundary layers at the cathode surface decreases, which, in turn, increases the flux of CO_2 to the cathode surface. As a result, the $m/z = 44$ mass-ion current signal increases with electrolyte flow rate (see SI-11). As the hydrodynamic boundary layer thickness is reduced, the H_2 partial current density decreases and the CO partial current density increases at a fixed potential, as shown in Figure 5A (see SI-12). Similar trends are observed over polycrystalline Ag thin films in a traditional H-cell when the
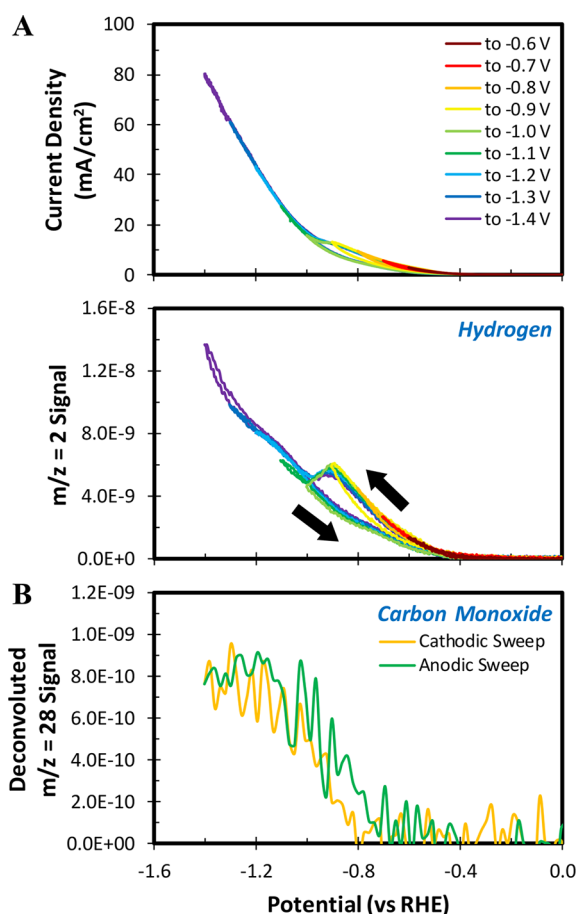
Figure 7. (A) H_2 evolution activity of Cu during CO_2 reduction measured during cyclic voltammetry to a series of increasingly cathodic vertex potentials at a scan rate of 20 mV/s in 0.1 M $CsHCO_3$ at a flow rate of 85 mL/min. The black arrows indicate the scan direction. (B) CO evolution activity of Cu measured during cyclic voltammetry at a scan rate of 1 mV/s in 0.1 M $CsHCO_3$ at a flow rate of 85 mL/min. Note that the onset and plateau of CO evolution correspond to the onset and saturation point, respectively, of the observed hysteresis in the rate of H_2 evolution over Cu during CO_2 reduction.

products are quantified by GC (see SI-13). As the hydrodynamic boundary layer thickness increases, the local pH should increase at a fixed current density, leading to CO_2 depletion by acid−base reaction at more anodic potentials.[7] To validate this hypothesis, the mass-ion current signal associated with CO_2 was plotted as a function of the deconvoluted mass-ion current signal associated with CO for each linear potential sweep performed. Figure 5B shows that as the electrolyte flow rate is increased, the point at which the CO_2 signal rapidly declines shifts to higher CO evolution rates, which correspond to increasingly cathodic potentials. These results demonstrate the ability of the DEMS approach to explain observed activity trends based on the composition of the local reaction environment in the immediate vicinity of the cathode.

CO_2 Reduction over Cu. Carbon dioxide ($m/z = 44$), hydrogen ($m/z = 2$), methane ($m/z = 15$), and ethene ($m/z = 26$) are the only reaction products produced over Cu that generate a unique mass fragment upon ionization (see SI-14). Formic acid is undetectable because it does not pervaporate. However, carbon monoxide can be detected after deconvoluting the mass-ion current for $m/z = 28$, which also contains contributions from CO_2 and ethene. The primary C_3 products
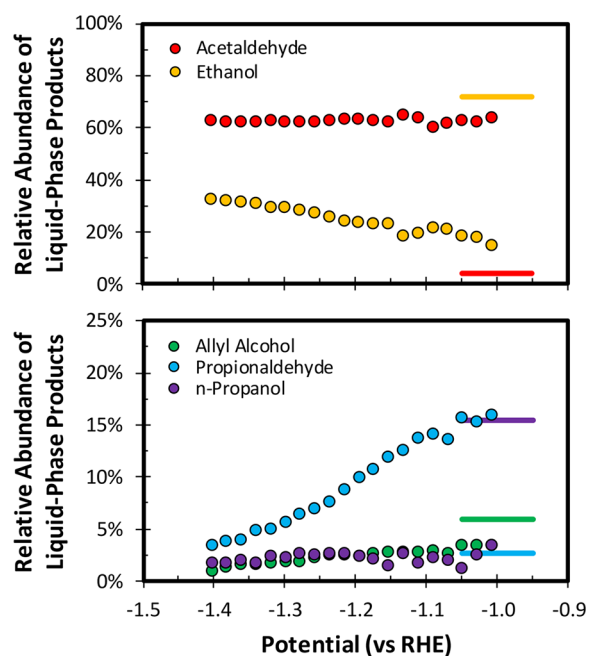

Figure 8. Observed relative abundance of the liquid-phase products produced over Cu during cyclic voltammetry at a scan rate of 1 mV/s in 0.1 M $CsHCO_3$ at a flow rate of 85 mL/min. The solid lines represent the relative molar abundances of the liquid phase products produced over Cu during chronoamperometry at −1 V vs RHE in a traditional H-cell when analyzing the bulk electrolyte.

produced over Cu are allyl alcohol, propionaldehyde, and n-propanol, each of which generate a series of unique mass fragments at $m/z = 57$, 58, and 59 upon ionization. As a result, the extent to which each of these products contributes to the observed mass spectrum can be calculated by solving a system of linear equations (see SI-15). Once this is accomplished, the contribution of the C_3 products to the remaining mass-ion currents can be accounted for. Acetaldehyde and ethanol produce a series of mass fragments upon ionization at $m/z = 31$ and 43 that are also unique once the contributions of the C_3 products have been accounted for. Thus, the contributions of acetaldehyde and ethanol to the observed mass spectrum can also be calculated by solving a system of linear equations. Using this approach, the complete deconvolution of the observed mass spectrum can be conducted, enabling 10 different relevant species to be detected in real time during cyclic voltammetry, as shown in Figure 6. While the deconvoluted mass-ion current signals are directly proportional to the generation rates of the corresponding reaction products, quantifying the partial current densities of these products on the basis of the deconvoluted signal is not possible due to the lack of a calibration protocol analogous to the method employed over Ag. Furthermore, alternative calibration protocols, such as flowing a standard gas mixture into the mass spectrometer, would not be accurate, because the observed mass-ion currents are dependent on the flux of each product into the mass spectrometer, which is a convolution of the generation rate and collection efficiency for each species.

It is notable that the product distribution observed over Cu during cyclic voltammetry displays hysteresis between the cathodic and anodic sweeps. This hysteresis is characterized by an enhanced generation rate of multicarbon products at the expense of hydrogen and methane during the anodic sweep. The hysteresis cannot be attributed to discrepancies in the local
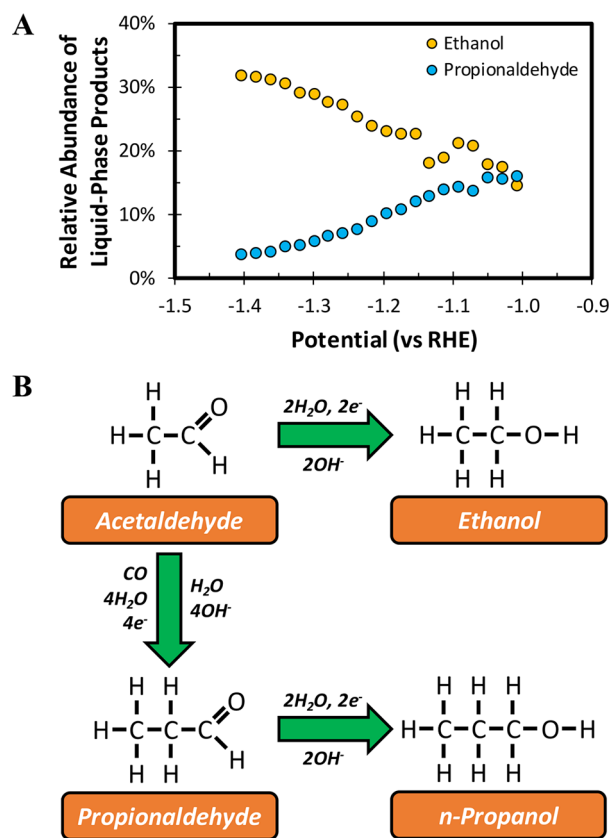
A

B

Figure 9. (A) Enhanced relative abundance of ethanol at the expense of propionaldehyde observed over Cu during cyclic voltammetry at a scan rate of 1 mV/s in 0.1 M $CsHCO_3$ at a flow rate of 85 mL/min. (B) Proposed mechanism of C_2 and C_3 primary alcohol formation over Cu from an acetaldehyde intermediate.

CO_2 concentration as the CO_2 signal is identical in both scan directions. To determine whether the hysteresis is potential dependent, cyclic voltammetry was conducted to a series of increasingly cathodic vertex potentials while monitoring the $m/z = 2$ mass-ion current. As shown in Figure 7A, hysteresis only occurs upon polarization to potentials more cathodic than −0.8 V vs RHE. As shown in Figure 7B, this potential agrees well with the potential at which CO is first observed by mass spectrometry. Furthermore, the hysteresis saturates at −1 V vs RHE, where the rate of CO evolution over Cu is observed to plateau. It has been proposed previously that hysteresis of the voltammogram is a result of CO accumulation on the Cu surface.[19,20] While the product distribution hysteresis observed over Cu during cyclic voltammetry has not been reported previously, the results obtained here are in agreement with the hypothesis that the hysteresis is caused by the accumulation of CO on the Cu surface. The rate of multicarbon product formation is higher during the anodic sweep because polarization to more cathodic potentials results in an elevated coverage of CO on the Cu surface that persists long enough to significantly impact the activity of Cu during the anodic sweep. To confirm this hypothesis, the transient activity of Cu was measured at −1 V vs RHE before and after polarization to −1.4 V vs RHE (see SI-16). After polarization to −1.4 V vs RHE, the ethene signal ($m/z = 26$) observed at −1 V vs RHE was ∼20% higher than that before the brief cathodic polarization. Furthermore, the enhanced activity took over 5 min to decay back to the value observed before the brief cathodic

polarization to −1.4 V vs RHE. Thus, it seems likely that the observed product distribution hysteresis is caused by the accumulation of CO on the Cu surface, which takes several minutes to reach steady state once the extent of cathodic polarization is reduced.

To determine the relative generation rates of the liquid-phase products, the differences in their relative volatilities must be accounted for. This can be accomplished by normalizing the deconvoluted signal for each product by the signal observed upon analysis of a standard solution with a fixed concentration. As shown in Figure 8, the relative abundance of the liquid-phase products observed by DEMS is significantly different from what is typically observed over Cu when the liquid-phase products are sampled from the bulk electrolyte. Acetaldehyde and propionaldehyde are produced with a 2−4 times higher abundance than ethanol or n-propanol. Conversely, the ethanol and n-propanol are typically produced with a molar abundance roughly an order of magnitude higher than that of the corresponding aldehydes.[19,21] While it has been demonstrated that the electrochemical reduction of these aldehydes produces the corresponding alcohols,[9,22] this is not sufficient evidence to conclude that they are transiently produced during CO_2 reduction over Cu. However, by collecting products at the electrode−electrolyte interface, these extremely volatile inter-mediate reaction products can be observed, suggesting that these aldehydes are relatively abundant within the local reaction environment but are typically reduced further to the corresponding primary alcohols before diffusing into the bulk electrolyte. To confirm that the pervaporate contains a high concentration of aldehydes relative to alcohols, chronoamperometry was conducted at −1.3 V vs RHE for 200 min while the pervaporate was passed through a condenser cooled with liquid N_2. The condensate was collected and analyzed by HPLC, which confirmed the high concentration of aldehydes relative to alcohols in the pervaporate (see SI-17). The concentration of aldehydes and alcohols in the recirculated catholyte was found to be negligible, confirming the high collection efficiency for the liquid-phase products. Interestingly, the relative abundance of ethanol increases at the expense of propionaldehyde at more cathodic potentials, as shown in Figure 9A. This novel observation suggests that ethanol and propionaldehyde share a common intermediate, such as acetaldehyde. This proposed mechanism is shown in Figure 9B. As the potential becomes increasingly cathodic, the electrochemical reduction of acetaldehyde to ethanol is expected to become increasingly exergonic relative to the chemical C−C coupling between acetaldehyde and CO, which is hypothesized to lead to propionaldehyde formation.[8,23] Thus, the observed liquid-phase product selectivity potential dependence can be rationalized on the basis of both reaction products being derived from an acetaldehyde intermediate.

■ CONCLUSIONS

We have demonstrated that the local reaction environment during the electrochemical reduction of CO_2 can be observed and quantified using a DEMS cell in which the catalyst is deposited directly onto the pervaporation membrane. We have shown that for CO_2 reduction over Ag, the amounts of H_2 and CO generated agree very well with what is observed by gas chromatographic analysis of the effluent from an H-cell operated with the same catalyst and electrolyte. Furthermore, we have observed the reaction of CO_2 with hydroxyl anions evolved at the cathode surface and have demonstrated that the

influence of this relatively slow chemical reaction on the measured electrocatalytic activity of Ag can be minimized by conducting product analysis during a rapid potential sweep. We have also shown how mass transfer to and from the catalyst influences the composition of the local reaction environment and measured electrocatalytic activity of Ag. For the electrochemical reduction of CO_2 over Cu, we have detected nine products continuously during cyclic voltammetry, which led to the observation of a potential-dependent hysteresis of the product distribution that favors multicarbon product generation during the anodic sweep. Finally, we have discovered that the electrolyte in contact with the cathode has a much higher concentration of aldehydes (acetaldehyde and propionaldehyde) than the corresponding alcohols (ethanol and n-propanol). We have also observed that at more cathodic potentials the concentration of ethanol near the cathode increases as the expense of propionaldehyde. These observations suggest acetaldehyde is a precursor to ethanol and propionaldehyde, and that the latter is a precursor to n-propanol.

ASSOCIATED CONTENT

Supporting Information

The Supporting Information is available free of charge on the ACS Publications website at DOI: 10.1021/jacs.8b04058.

SI-1, optimization of the metallic thin film thickness; SI-2, validating surface purity by X-ray photoelectron and ion-scattering spectroscopies; SI-3, quantifying the uncompensated resistance of the DEMS cell; SI-4, quantifying the relative electrochemical surface area of the DEMS electrode; SI-5, mass spectra of reactants and products; SI-6, H_2 calibration procedure; SI-7, H_2 evolution linear sweep voltammetry over Ag versus scan rate; SI-8, calculated signal contributions over Ag; SI-9, CO calibration procedure; SI-10, linear sweep voltammetry over Ag versus scan rate; SI-11, CO_2 signal versus flow rate; SI-12, linear sweep voltammetry over Ag versus electrolyte flow rate; SI-13, chronoamperometry staircase over Ag versus CO_2 flow rate in an H-cell; SI-14, calculated signal contributions over Cu; SI-15, deconvolution of the mass-ion currents observed over Cu; SI-16, transient ethene generation rate before and after cathodic polarization; and SI-17, analysis of the pervaporate collected over Cu by liquid chromatography (PDF)

AUTHOR INFORMATION

Corresponding Author

*alexbell@berkeley.edu

ORCID

Alexis T. Bell: 0000-0002-5738-4645

Notes

The authors declare no competing financial interest.

ACKNOWLEDGMENTS

REFERENCES

(1) Jitaru, M.; Lowy, D. A.; Toma, M.; Toma, B. C.; Oniciu, L. *J. Appl. Electrochem.* **1997**, *27* (8), 875−889.

(2) Gattrell, M.; Gupta, N.; Co, A. *J. Electroanal. Chem.* **2006**, *594* (1), 1−19.

(3) Hori, Y. Electrochemical CO_2 Reduction on Metal Electrodes. In *Modern Aspects of Electrochemistry*; Vayenas, C. G., White, R. E., Gamboa-Aldeco, M. E., Eds.; Springer: New York, 2008; pp 89−189.

(4) Hori, Y.; Kikuchi, K.; Suzuki, S. *Chem. Lett.* **1985**, *14* (11), 1695−1698.

(5) Noda, H.; Ikeda, S.; Oda, Y.; Imai, K.; Maeda, M.; Ito, K.; Ideka, S.; Oda, Y.; Imai, K.; Maeda, M.; et al. *Bull. Chem. Soc. Jpn.* **1990**, *63* (9), 2459−2462.

(6) Gupta, N.; Gattrell, M.; MacDougall, B. *J. Appl. Electrochem.* **2006**, *36* (2), 161−172.

(7) Singh, M. R.; Clark, E. L.; Bell, A. T. *Phys. Chem. Chem. Phys.* **2015**, *17* (29), 18924−18936.

(8) Garza, A.; Bell, A. T.; Head-Gordon, M. *ACS Catal.* **2018**, *8*, 1490−1499.

(9) Schouten, K. J. P.; Kwon, Y.; van der Ham, C. J. M.; Qin, Z.; Koper, M. T. M. *Chem. Sci.* **2011**, *2* (10), 1902−1909.

(10) Bertheussen, E.; Verdaguer-Casadevall, A.; Ravasio, D.; Montoya, J. H.; Trimarco, D. B.; Roy, C.; Meier, S.; Wendland, J.; Nørskov, J. K.; Stephens, I. E. L.; et al. *Angew. Chem., Int. Ed.* **2016**, *55* (4), 1450−1454.

(11) Wolter, O.; Heitbaum, J. *Berichte der Bunsengesellschaft fur Phys. Chemie* **1984**, *88* (1), 2−6.

(12) Baltruschat, H. *J. Am. Soc. Mass Spectrom.* **2004**, *15* (12), 1693−1706.

(13) Clark, E. L.; Singh, M. R.; Kwon, Y.; Bell, A. T. *Anal. Chem.* **2015**, *87* (15), 8013−8020.

(14) Wuttig, A.; Surendranath, Y. *ACS Catal.* **2015**, *5* (7), 4479−4484.

(15) Resasco, J.; Lum, Y.; Clark, E. L.; Zeledon, J.; Bell, A. T. *ChemElectroChem* **2018**, *5*, 1−10.

(16) Hoshi, N.; Kato, M.; Hori, Y. *J. Electroanal. Chem.* **1997**, *440* (1−2), 283−286.

(17) Hatsukade, T.; Kuhl, K. P.; Cave, E. R.; Abram, D. N.; Jaramillo, T. F. *Phys. Chem. Chem. Phys.* **2014**, *16* (27), 13814−13819.

(18) Firet, N. J.; Smith, W. A. *ACS Catal.* **2017**, *7* (1), 606−612.

(19) Hori, Y.; Murata, A.; Takahashi, R. *J. Chem. Soc., Faraday Trans. 1* **1989**, *85* (8), 2309−2326.

(20) Hori, Y.; Murata, A.; Yoshinami, Y. *J. Chem. Soc., Faraday Trans.* **1991**, *87* (1), 125−128.

(21) Kuhl, K. P.; Cave, E. R.; Abram, D. N.; Jaramillo, T. F. *Energy Environ. Sci.* **2012**, *5* (5), 7050−7059.

(22) Hori, Y.; Takahashi, R.; Yoshinami, Y.; Murata, A. *J. Phys. Chem. B* **1997**, *101* (36), 7075−7081.

(23) Goodpaster, J. D.; Bell, A. T.; Head-Gordon, M. *J. Phys. Chem. Lett.* **2016**, *7* (8), 1471−1477.